

# The amplified second outbreaks of global COVID-19 pandemic

Jianping Huang<sup>1,\*</sup>, Xiaoyue Liu<sup>1</sup>, Li Zhang<sup>1</sup>, Kehu Yang<sup>2</sup>, Yaolong Chen<sup>2</sup>,  
Zhongwei Huang<sup>1</sup>, Chuwei Liu<sup>1</sup>, Xinbo Lian<sup>1</sup>, Danfeng Wang<sup>1</sup>

<sup>1</sup>Collaborative Innovation Center for Western Ecological Safety,  
Lanzhou University, Lanzhou, 730000, China.

<sup>2</sup>Evidence-based Medicine Center, Lanzhou University, Lanzhou, 730000, China

\* Correspondence author: Jianping Huang (hjp@lzu.edu.cn)

## Abstract

COVID-19 is now in an epidemic phase, with a second outbreak likely to appear at any time. The intensity and timing of a second outbreak is a common concern worldwide. In this study, we made scenario projections of the potential second outbreak of COVID-19 using a statistical-epidemiology model, which considers both the impact of seasonal changes in meteorological elements and human social behaviors such as protests and city unblocking. Recent street protests in the United States and other countries are identified as a hidden trigger and amplifier of the second outbreak. The scale and intensity of subsequent COVID-19 outbreaks in the U.S. cities where the epidemic is under initial control are projected to be much greater than those of the first outbreak. For countries without reported protests, lifting the COVID-19 related restrictions prematurely would accelerate the spread of the disease and place mounting pressure on the local medical system that is already overloaded. We anticipate these projections will support public health planning and policymaking by governments and international organizations.

## 28 **1 Introduction**

29       Recently, the COVID-19 pandemic has spread rapidly and poses a dire threat to global  
30 public health, which claimed over 0.49 million lives, along with 9.8 million confirmed  
31 cases as of June 28<sup>th</sup><sup>1</sup>. Beyond the spread itself, the outbreak may have far-reaching  
32 consequences, negatively affecting the economic development worldwide and posing a  
33 series of long-standing social problems<sup>2,3</sup>. There is an urgent need for a global prediction  
34 system that can provide scientific guidelines for the World Health Organization and  
35 international decision-makers to implement effective containment measures capable of  
36 curbing the spread of COVID-19<sup>4</sup>. Researchers worldwide have developed various models  
37 with mathematical and statistical methods, including stochastic simulations, lognormal  
38 distribution<sup>5</sup>, machine learning, and artificial intelligence<sup>6</sup>. Among them, the  
39 susceptible-infectious-removed infectious disease model (SIR) is the most widely used<sup>7-9</sup>.  
40 However, this simple model is built under a series of idealized assumptions, which may  
41 limit the accuracy and reliability of the prediction. In order to obtain the prediction results  
42 with higher credibility, more complex models with fewer assumptions should be developed  
43 so as to simulate the actual situations in a more realistic manner<sup>10</sup>.

44       Although it is difficult to establish an accurate epidemiological model describing the  
45 spread of a pandemic, the reported global pandemic data contain particular solutions to the  
46 mathematical equations incorporated in epidemiological models<sup>3,6</sup>. It is theoretically  
47 possible to remedy the defects of prior epidemiological models by introducing the latest  
48 pandemic data and hence improve the pandemic prediction<sup>2,4,6</sup>. Based on this idea, we have  
49 developed a Global Prediction System of the COVID-19 Pandemic (GPCP)<sup>11</sup>. The system  
50 develops a modified version of the SIR model and determines the parameters through  
51 historical data fitting<sup>12,13</sup>, which allows it to make targeted predictions for various countries  
52 and obtain better prediction results. The first version of GPCP (CPCP-1) can capture the  
53 major features of the daily number of confirmed new cases and provides reliable  
54 predictions. However, the prediction of GPCP-1 is only valid for one month<sup>11</sup>.

55 In this study, the second version of the Global Prediction System for COVID-19  
56 Pandemic (GPCP-2) is developed based on a modified SEIR model<sup>14</sup>. The system considers  
57 both the seasonal changes of meteorological elements and human social behaviors  
58 including protests and city unblocking. The paper is arranged as follows: the details of the  
59 datasets and the methodology used are given in section 2. In section 3, projections of 12  
60 cities in the United States are presented. The projections of 15 countries with reported  
61 protests and 15 countries without reported protests are shown in section 4 and section 5,  
62 respectively. Discussion and conclusion are presented in section 6.

## 63 **2 Method**

### 64 2.1 The modified SEIR model

65 The second version of Global Prediction System for COVID-19 Pandemic (GPCP) is  
66 built based on a modified SEIR model<sup>15</sup>. The traditional SEIR model<sup>10,14</sup> defines seven  
67 states of the disease: susceptible cases (S), insusceptible cases (P), potentially infected  
68 cases (E, infected cases in a latent period), infectious cases (I, infected cases that have not  
69 been quarantined), quarantined cases (Q, confirmed and quarantined cases), recovered  
70 cases (R), and cases of mortality (D). The SEIR model is able to emulate the time curve of  
71 an outbreak. The model is consisted of the following equations:

$$72 \quad \frac{dS(t)}{dt} = -\beta(t)I(t)S(t)/N - \alpha S(t) , \quad (1)$$

$$73 \quad \frac{dP(t)}{dt} = \alpha S(t) , \quad (2)$$

$$74 \quad \frac{dE(t)}{dt} = \beta(t)I(t)S(t)/N - \gamma(t)E(t) , \quad (3)$$

$$75 \quad \frac{dI(t)}{dt} = \gamma(t)E(t) - \delta(t)I(t) , \quad (4)$$

$$76 \quad \frac{dQ(t)}{dt} = \delta(t)I(t) - \lambda(t)Q(t) - \kappa(t)Q(t) \quad (5)$$

$$77 \quad \frac{dR(t)}{dt} = \lambda(t)Q(t) \quad (6)$$

$$78 \quad \frac{dD(t)}{dt} = \kappa(t)Q(t) \quad (7)$$

79 The sum of the six categories is equal to the total population (N) at any time.

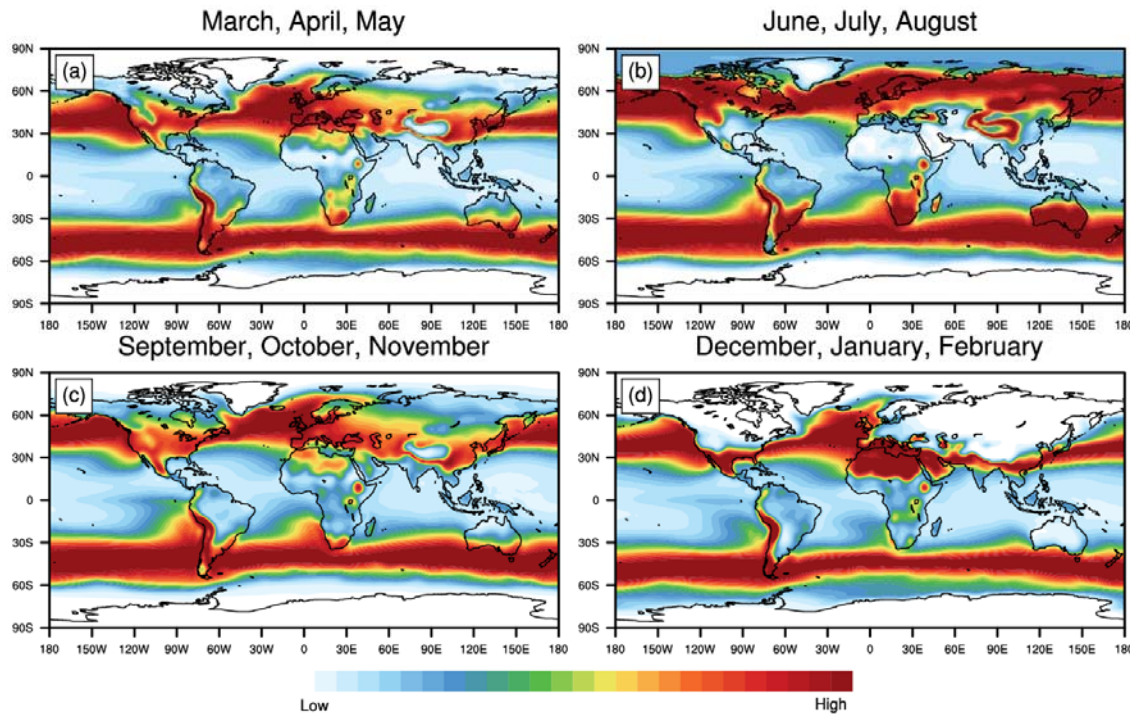
$$80 \quad S + P + E + I + Q + R + D = N$$

81 We modified the model by introducing the timing of community reopening collected  
82 from news reports. If the timing collected from news reports is not explicit enough as an  
83 input to our model, the timing will be indicated by the daily new cases on the day of  
84 reopening ( $dQ_c$ ). As the number of newly confirmed cases on a given day falls lower than  
85  $dQ_c$ , local authority begins to lift or loose the lockdowns.

86 In addition, the temporal variation of transmission rate due to changes in local  
87 temperature as well as human behaviors are considered. Generally, the transmission rate  
88 ( $\beta(t)$ ) can be expressed by the following equations:

$$\beta(t) = \begin{cases} \beta_0 & t < t_{int} \\ \beta_1 & t_{int} \leq t < t_{lift} \\ \beta_2 + E \times F(t) & t \geq t_{lift} \end{cases}$$

89 where  $\beta_0$  represents the transmission rate in the non-intervention period at the early stage  
90 of the pandemic ( $t < t_{int}$ );  $\beta_1$  represents the transmission rate during the intervention  
91 period ( $t_{int} \leq t < t_{lift}$ );  $\beta_2$  represents the transmission rate after the restriction is lifted.  
92  $\beta_0$  and  $\beta_1$  are fitted against the actual reported data, while  $\beta_2$  is the assumed value in  
93 possible future scenarios. We assume a 14-day delay in the effect of the intervention on the  
94 infection rate.  $F(t)$  is the PDF function obtained by Huang et al.<sup>16</sup>, who found that 60.0%  
95 of confirmed COVID-19 cases occurred in places where the air temperature ranged from  
96 5°C to 15°C. Using the NCEP reanalysis data, we calculated the global distribution of  
97 probability distribution function (PDF) values on each day of the year and included its  
98 influence on the infection rate. Figure 1 shows the PDF values for the four seasons in a year.  
99 High PDF values correspond to the ambient temperature that is conducive for the virus to  
100 spread. For the northern hemisphere, the optimal band generally moves northward in  
101 summer (June, July, and August) and moves southward in winter (December, January, and  
102 February), while for southern hemisphere the optimal band moves southward in summer  
103 (December, January, and February) and moves northward in winter (June, July, and  
104 August).



105

106 **Figure 1: The optimal temperature zone for the spread COVID-19.** Regions with warm  
107 shadings indicate more conducive temperature for the spread of the virus and vice versa.

108 Since the seasonality of transmission is still disputed and future trajectory of the  
109 outbreaks may be influenced by the intensity of intervention measures, four future  
110 scenarios are designed to project the epidemic after easing COVID-19 related restrictions:

111 - **Scenario 1:** The restrictions are completely lifted after  $t_{int}$  ( $\beta_2 = \beta_0$ ). The seasonal  
112 forcing on the transmission rate is considered ( $E = 1$ ).

113 - **Scenario 2:** The restrictions are partially lifted after  $t_{int}$  ( $\beta_2 = (\beta_0 + \beta_1)/2$ ). The  
114 seasonal forcing on the transmission rate is considered ( $E = 1$ ).

115 - **Scenario 3:** The restrictions are completely lifted after  $t_{int}$  ( $\beta_2 = \beta_0$ ). The seasonal  
116 forcing on the transmission rate is not considered ( $E = 0$ ).

117 - **Scenario 4:** The restrictions are partially lifted after  $t_{int}$  ( $\beta_2 = (\beta_0 + \beta_1)/2$ ). The  
118 seasonal forcing on the transmission rate is not considered ( $E = 0$ ).

## 119 2.2 Parameter fitting and numerical solutions

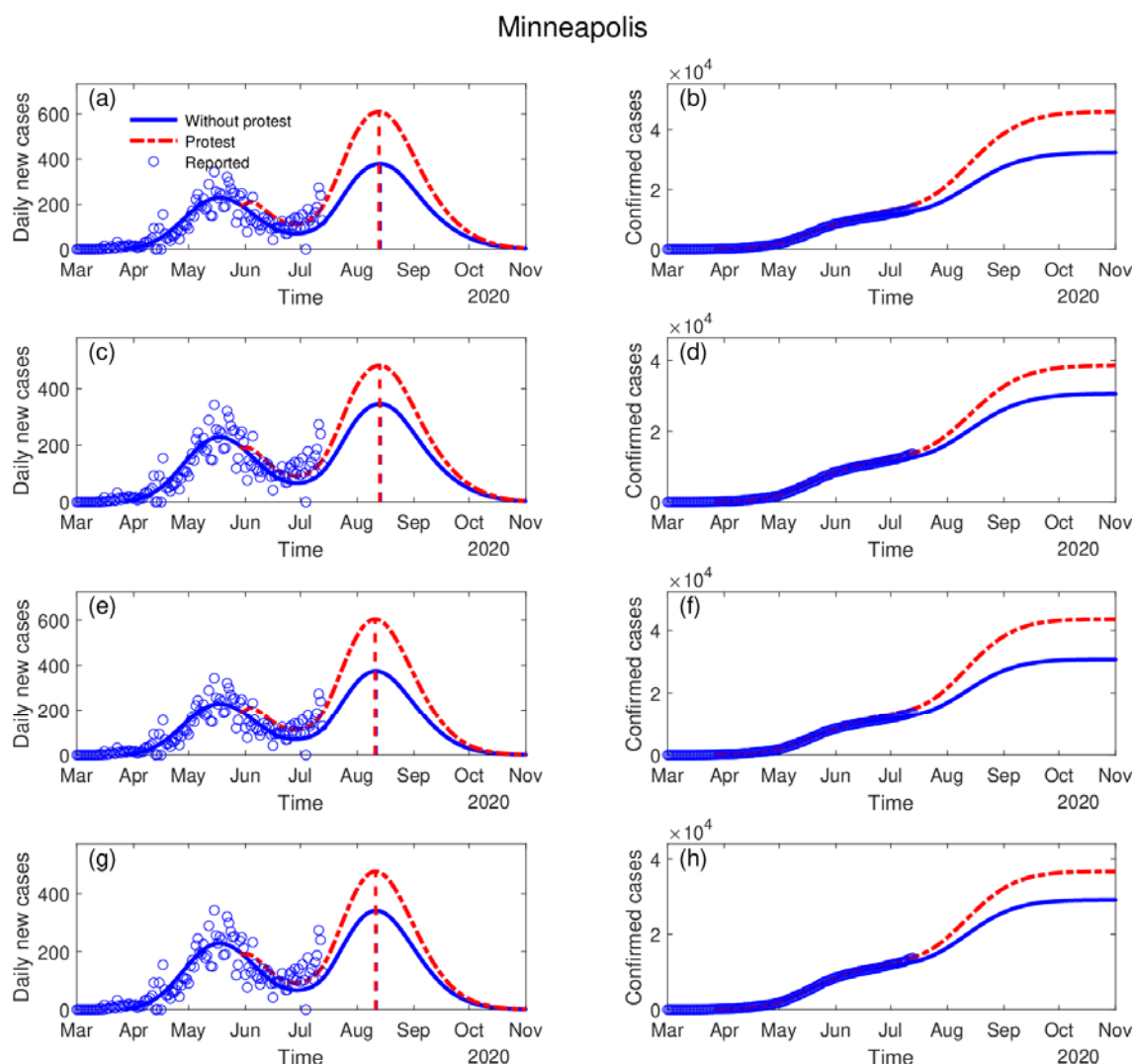
120 In order to enhance the stability of the traditional least square method (Gauss-Newton  
121 algorithm), we use an improved damped least square method called Levenberg-Marquardt

122 algorithm<sup>17</sup>. This method inserts a damping coefficient into the Gauss-Newton method  
123 when calculating the Hessian matrix. The benefit of introducing this damping coefficient is  
124 that it can converge very quickly in the steepest direction in many cases even when the  
125 initial solution is very far from ideal values, which makes the parameter determination  
126 more robust<sup>18</sup>. In addition, for all damping coefficient greater than 0, the coefficient matrix  
127 is positive definite which makes the Hessian matrix in the descending direction. The input  
128 variables to obtain fitted parameters ( $\alpha$ ,  $\beta$ ,  $\gamma$ ,  $\delta$ ,  $\lambda$ , and  $\kappa$ ) are the time series of confirmed  
129 ( $Q(t) - D(t) - R(t)$ ), death ( $D(t)$ ), and recovered ( $R(t)$ ) cases provided by from Johns  
130 Hopkins University Center for Systems Science and Engineering<sup>1</sup>. The equations are solved  
131 using the classic 4th order Runge-Kutta method.

### 132 **3 Projections of the US cities**

133 Unfortunately, the recent protests against police violence in cities across the United  
134 States have gone ahead despite the current rising COVID-19 pandemic and potential  
135 subsequent outbreaks, possibly with higher intensity. Large public gatherings, shouting, and  
136 marching shoulder to shoulder may have already sown the seeds of the second outbreaks in  
137 regions under initial control<sup>19,20</sup> and made it even more difficult to contain the epidemic in  
138 regions where the curve is still increasing. The use of tear gas and pepper spray against the  
139 protesters may also have produced violent coughing and runny noses, forcing protesters to  
140 remove their masks and making the crowds even more susceptible to the virus. A certain  
141 number of patients with the latent disease may have participated in the protests and spread  
142 the disease to healthy protesters, police officers, and national guards who are not yet  
143 immune to the virus<sup>21</sup>. If the close contacts of the infectious are not fully tracked, they may  
144 spread the virus to other groups of people, increasing the risk of a larger size of outbreaks.  
145 Here, we simulated the impact of large-scale protests on the potential second outbreaks in  
146 several cities of the United States<sup>22</sup> (Figure 2 and Table 1). The model generally predicted a  
147 second wave of COVID-19 in the second half of 2020. We estimated the increase in the  
148 population of potentially infected people ( $\delta E_t$ ) for each city based on the ratio of the

149 number of infected persons ( $Q_t$ ) to the total population of the city ( $N$ ). The timing of  
150 protests and the number of protesters in each city were collected from local news reports  
151 (Table 1). The increase in the population of potentially infected people ( $\delta E_t$ ) and the  
152 populations of protesters ( $\delta S_t$ , regarded as an increase in the population of susceptible)  
153 were used as the force input for the model calculations to simulate the impact of protests on  
154 the outbreaks. When the protests begin, we force group E and group S to increase  $\delta E_t$  and  
155  $\delta S_t$ , respectively.



156

157 **Figure 2: The impact of protests on the possible second outbreak in Minneapolis.** The  
158 blue dots denote the reported daily incidence of COVID-19 cases. The blue line represents  
159 the simulation and projections without protests, while the dashed red line denotes the  
160 simulation and projections with protests. Four scenarios with protests and four scenarios



161 without protests are simulated. (a)~ (b), (c)~(d), (e)~(f), (g)~(h) are the simulation for  
162 Scenario 1, 2, 3, 4, respectively. (a)~(b) and (c)~(d) are the simulations with seasonal  
163 forcing; (e)~(f) and (g)~(h) are the simulations without seasonal forcing. (a)~(b) and (e)~(f)  
164 are the simulations where the restrictions are completely lifted; (c)~(d) and (g)~(h) are the  
165 simulations where the restrictions are partially lifted.

166 Figure 2 shows the projections for Minneapolis in 8 scenarios (4 scenarios with protests  
167 and 4 without). After the COVID-19 restrictions were lifted, an upward trend of daily new  
168 cases has been observed. The protests would significantly amplify the intensity of the  
169 second outbreak but may not be able to advance it. In scenarios 1, the second outbreak of  
170 Minneapolis will peak in mid-August 2020. The comparison between scenarios indicates  
171 that the effect of intervention measures outweighs the seasonal forcing. For the rest of the  
172 12 cities, the model also predicted enhanced second outbreaks when the impact of protests  
173 is considered (Table 1). Due to space constraints, the details of the projection results are not  
174 presented in the manuscript and can be accessed at <http://covid-19.lzu.edu.cn/>.  
175

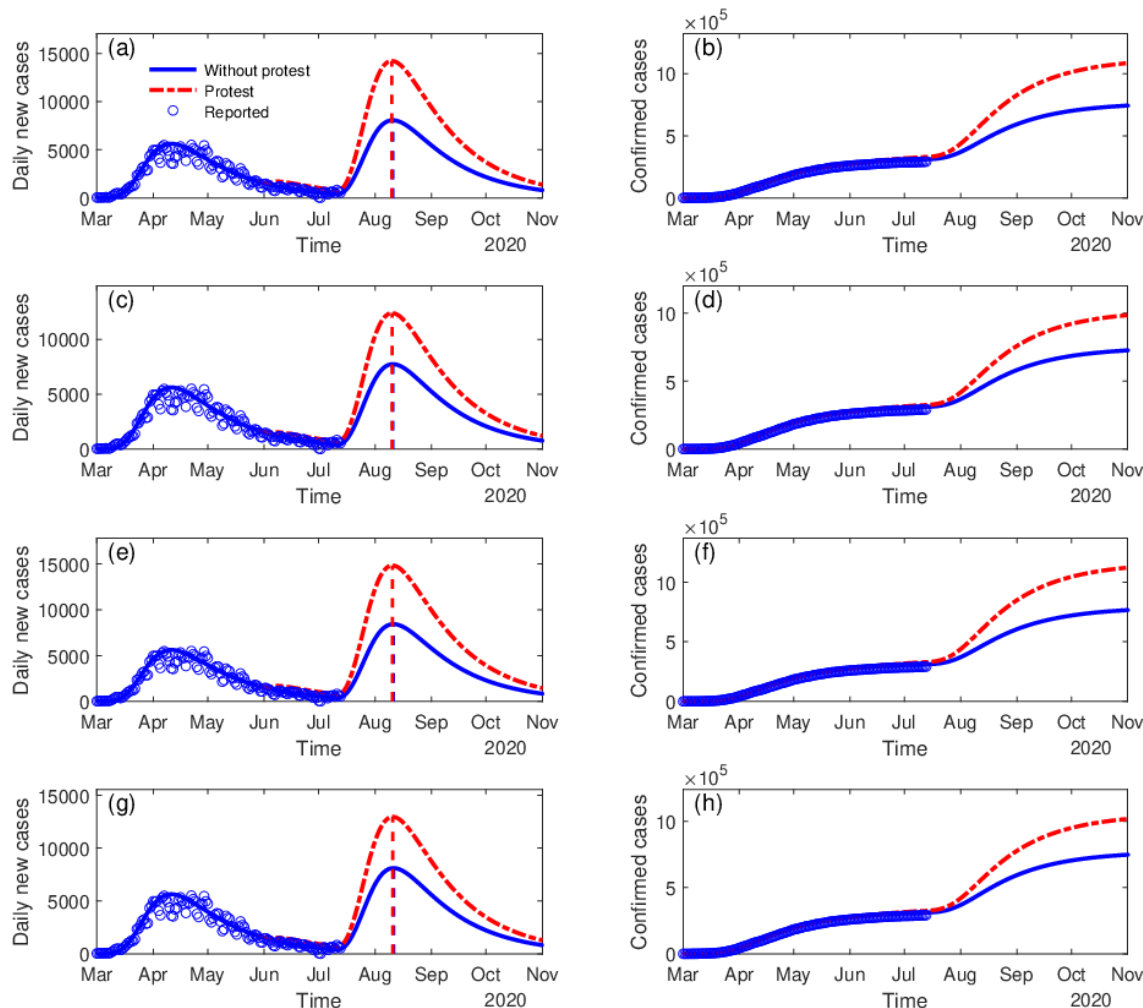


176 **Table 1 Projections of the second outbreaks in some US cities in Scenario 1**

Countries	Population (million)	Start date of Protests	Estimated participants	The peak time of the second outbreaks	Peak time daily new incidence without protests	Peak time daily new incidence with protests	End of the second outbreak	Accumulated Confirmed Cases
New York City (New York)	8.33	May, 29 <sup>th</sup>	25,000	Mid-August	Around 8,000	Around 18,000	End of 2020	Around 900,000
Chicago (Illinois)	5.15	May, 28 <sup>th</sup>	30,000	Mid-September	Around 2700	Around 4100	End of 2020	Around 390,000
Minneapolis (Minnesota)	1.26	May, 26 <sup>th</sup>	30,000	Mid-September	Around 400	Around 700	End of 2020	Around 48,000
Columbus (Ohio)	1.31	May, 28 <sup>th</sup>	10,000	Late-September	Around 120	Around 380	End of 2020	Around 35,000
Westchester (Illinois)	0.97	May, 29 <sup>th</sup>	30,000	Mid-August	Around 3,500	Around 5,500	September, 2020	Around 150,000
Philadelphia (Pennsylvania)	10.04	May, 30 <sup>th</sup>	10,000	Mid-October	Around 800	Around 1,700	End of 2020	Around 120,000
Seattle (Washington)	2.25	May, 29 <sup>th</sup>	50,000	Late-August	Around 2,00	Around 600	End of 2020	Around 35,000
Washington, D.C.	0.70	May, 29 <sup>th</sup>	10,000	Mid-October	Around 180	Around 650	September, 2020	Around 70,000
San Francisco (California)	0.88	May, 30 <sup>th</sup>	30,000	Mid-August	Around 100	Around 400	October, 2020	Around 22,000
Detroit (Michigan)	1.75	May, 29 <sup>th</sup>	30,000	Early-September	Around 1,000	Around 2,200	October, 2020	Around 70,000
Miami-Dade (Florida)	2.72	May, 30 <sup>th</sup>	20,000	Mid-August	Around 1,800	Around 3,000	September, 2020	Around 120,000
San Diego (California)	3.34	May, 29 <sup>th</sup>	30,000	Late-August	Around 1,000	Around 1,600	September, 2020	Around 130,000

177 **4 Projections of countries with reported protests**

**United Kingdom**



178

179 **Figure 3: The impact of protests on the possible second outbreak in the United Kingdom.**

180 The blue dots denote the reported daily incidence of COVID-19 cases. The blue line  
181 represents the simulation and projections without protests, while the dashed red line denotes  
182 the simulation and projections with protests. The scenarios in these subplots are the same as  
183 Figure 2.

184 In addition to the United States, protests of a certain scale also broke out in other  
185 countries. Using similar parameterization of the protests, Table 3 presents the projections of  
186 the second outbreaks in the United Kingdom, the United States, Germany, Italy, Australia,  
187 Canada, Spain, Mexico, Switzerland, Belgium, Netherlands, Ireland, and Denmark. For the  
188 United Kingdom (Figure 3), the second outbreak is likely to peak during August. Under the

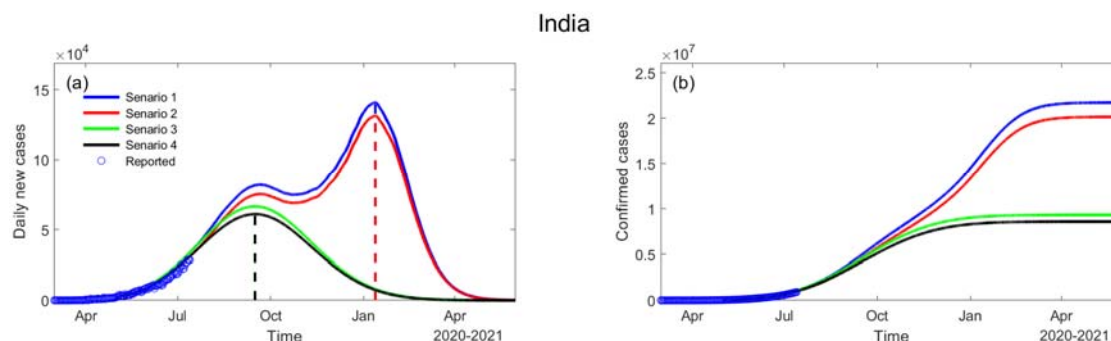
189 impact of protests, when the restrictions are lifted completely, a second wave with a peak of  
190 14,160 is expected, which is 75.6% higher than the scenario without protests (Scenario 1).  
191 The protests and the lifting of restrictions, along with the enhancement in the ability of virus  
192 transmission in the cold seasons due to temperature change may cause the recurrence of an  
193 outbreak that was initially under control. If the same intervention measures are implemented  
194 during the second outbreak, the second outbreak would be brought under control again by the  
195 end of 2020.

196 **Table 2 Projections of the second outbreaks in some countries (with protests)**

Countries	Population (million)	Start date of Protests	Estimated participants	The peak time of the second outbreaks	Peak time daily new incidence without protests	Peak time daily new incidence with protests	End of the second outbreak	Accumulated Confirmed Cases with protests
United Kingdom	66.48	May, 28 <sup>th</sup>	70,000	Early-August	Around 8,000	Around 14,170	End of 2020	Around 1,150,000
United States	328.2	May, 26 <sup>th</sup>	1,500,000	Late-July	Around 40,000	Around 120,000	End of 2020	Around 16,000,000
Germany	82.93	May 30 <sup>th</sup>	160,000	Early-September	Around 4,500	Around 7,000	End of 2020	Around 450,000
Italy	60.43	June, 30 <sup>th</sup>	150,000	Early-October	Around 6,000	Around 95,000	End of 2020	Around 600,000
Australia	25.44	June, 2 <sup>nd</sup>	14,000	Early-August	Around 500	Around 1,900	End of 2020	Around 45,000
Canada	37.05	May, 30 <sup>th</sup>	100,000	Late-September	Around 1,800	Around 2,500	End of 2020	Around 250,000
Spain	46.73	June, 1 <sup>st</sup>	10,000	Early-September	Around 7,600	Around 9,400	End of 2020	Around 1,100,000
Mexico	126.2	May, 30 <sup>th</sup>	50,000	Late-August	Around 5,800	Around 7,600	End of 2021	Around 1,500,000
Switzerland	8.57	May, 31 <sup>st</sup>	20,000	Early-August	Around 1,400	Around 2,100	October, 2020	Around 80,000
Belgium	11.42	June, 1 <sup>st</sup>	50,000	Late-August	Around 2,000	Around 4,200	End of 2020	Around 230,000
Netherlands	17.26	June, 1 <sup>st</sup>	56,000	Late-July	Around 1,800	Around 2,800	End of 2020	Around 170,000
Ireland	4.81	May, 31 <sup>st</sup>	20,000	Mid-July	Around 600	Around 1,500	End of 2020	Around 90,000
Denmark	5.73	May 31 <sup>st</sup>	20,000	Late-August	Around 600	Around 1,000	End of 2020	Around 60,000

197

## 198 5 Projections of countries without reported protest



199

200 **Figure 4: Projections of the second outbreak in India in different scenarios.** Scenarios 1  
201 and 2 are simulated with seasonal forcing, while scenarios 3 and 4 are simulated without  
202 seasonal forcing. Scenarios 1 and 3 are the projections where restrictions are fully lifted,  
203 while scenarios 2 and 4 are the projections where restrictions are partially lifted.

204 Mass gathering events during the epidemic should be restricted or even banned since  
205 they have the potential to enhance the second outbreak and pose further radical  
206 public-health challenges for health authorities and governments<sup>23,24</sup>. Lifting the restrictions  
207 too early may also have the potential to trigger subsequent outbreaks and further increase  
208 the pressure on the medical system. Fig 4 shows the projections of India in the four  
209 scenarios. With seasonal forcing, it is predicted that the first peak of the epidemic will  
210 occur in September while the second peak with higher intensity, caused environmental  
211 changes, will arrive in January 2021. Without seasonal forcing, there would be only one  
212 peak in September 2020. We also projected the epidemic curve for other countries  
213 including Russia, Brazil, Chile, etc. that are still in the rapid growing period. We classified  
214 them as ‘non-protesting countries’, not because there are no protests. Indeed, there might  
215 have been many protests and mass gatherings in India, Brazil, and other regions that may  
216 impact the outbreak on varying degrees, but the information on the timing and size of these  
217 protests are currently not available. Therefore, the role of these protests on the timing and  
218 size of the outbreaks can not be isolated and may not be incorporated as a force into the  
219 model.

220 From Table 3 we can see that the peak time and size of the second outbreak varies from  
221 countries to countries, due to different levels of interventions measures, environmental  
222 conditions, medical resources, etc. Regions with high population density are at higher risk  
223 of enhanced second outbreaks. When control measures are lifted too soon and  
224 environmental temperatures are more suitable for the spread of disease<sup>25</sup>, an enhanced  
225 second outbreak is expected. Therefore, when considering the timing of lifting the  
226 restrictions to restore the economy, it is necessary to analyze epidemic situations as well as  
227 climate factors. For example, during cold seasons when the transmission rate is higher,  
228 reopening would easily light up the second outbreaks, since conducive environmental  
229 factors and related human social behaviors (more frequent indoor gatherings) would,  
230 directly and indirectly, increase the transmission ability of the virus, leaving more people  
231 vulnerable to infection. Therefore, the peak of the second wave of the outbreak is most  
232 likely to synchronize with the fall of environmental temperature, displaying strong  
233 seasonality. During winter months, the temperate regions of the Northern and Southern  
234 Hemispheres experience highly synchronized annual influenza epidemics<sup>26</sup>. Additionally,  
235 when restrictions are lifted, personal protection (wearing face masks, keeping appropriate  
236 interpersonal distance, sterilization, etc)<sup>27</sup>. is still required or even mandatory in indoor  
237 places so as to minimize the infection rate by cutting off the infection routine.

**Table 3 Projections of the second outbreaks in some countries in Scenario 1 (without reported protests)**

Countries	Population (million)	The peak time of the second outbreaks	Peak time daily new incidence without protests	End of the second outbreak	Accumulated Confirmed Cases
India	1324	Early-November, 2020	Around 41,000	February, 2021	Around 6,000,000
Russia	144.5	Late-September, 2020	Around 12,000	April, 2021	Around 2,800,000
Brazil	209.5	Early-October, 2020	Around 60,000	February, 2021	Around 11,200,000
Peru	32.05	Late-October, 2020	Around 13,000	May, 2021	Around 2,500,000
Chile	18.60	Late-July, 2020	Around 11,000	April, 2021	Around 1,500,000
Argentina	44.49	January, 2021	Around 5000	April, 2021	Around 600,000
Pakistan	212.2	Early-August, 2020	Around 30,000	November, 2020	Around 2,700,000
Saudi Arabia	32.55	Late-July, 2020	Around 13,000	May, 2021	Around 3,500,000
Bangladesh	161.4	Late-August, 2020	Around 15,000	January, 2021	Around 1,600,000
Qatar	2.64	Early-September, 2020	Around 2,400	December, 2020	Around 240,000
Colombia	49.64	February, 2021	Around 12,500	May, 2021	Around 55,000
Belarus	9.51	Mid-August, 2020	Around 2,800	May, 2021	Around 2,800,000
Egypt	102.27	Mid-November, 2020	Around 2,800	March, 2021	Around 420,000
Ecuador	17.08	Mid-August, 2020	Around 5,000	December, 2020	Around 300,000



## 239 **6 Discussion and conclusion**

240 New treatments and vaccines are not yet available for any COVID-19-affected areas<sup>28</sup>.  
241 With the presence asymptomatic of carriers that may spread the virus, and the lack of herd  
242 immunity, a second outbreak is inevitable as confirmed cases of COVID-19 increase. Our  
243 results show that the timing and intensity of the second outbreaks are seasonally modulated  
244 and depend largely on local reopening policies. Higher seasonal variations in COVID-19  
245 transmission may lead to a greater incidence of recurrent wintertime outbreaks<sup>29</sup>. The  
246 current mass protests in the United States and other regions of the world could lead to  
247 amplified second outbreaks, overlapping the wintertime outbreaks and threatening more  
248 lives. This is because the extremely crowded environments facilitate the spread of the virus,  
249 leading to high rates of the second attack, as seen in both the 1918 pandemic and the 1957  
250 Asian influenza pandemic<sup>30-32</sup>.

251 If the transmission capacity of the second outbreak increases, it could place a  
252 catastrophic burden on the health system and create even more serious social and economic  
253 crises. However, if the chain of transmission is cut during the first outbreak, there will be  
254 no further outbreak similar to the first wave. The necessary drug therapies and vaccines  
255 currently require long-term development and testing, so nonpharmaceutical interventions  
256 are the only direct means available to suppress the spread of the disease<sup>33</sup>. In the face of a  
257 powerful pandemic, everyone must help to fight the virus. We must collectively follow the  
258 distancing limits recommended by global public-health organizations to effectively reduce  
259 the potential cost in the lives of the second wave of infection. Our findings should  
260 encourage close monitoring and early warning of the development of a global pandemic, as  
261 well as safeguards for our global prediction system to best contain the second wave<sup>34</sup>.  
262 These results provide a powerful scientific basis for governments to adjust their policies  
263 and control measures in real-time, to achieve the most effective allocation of medical  
264 resources before the second outbreak and to reduce the associated health risks.

265

266 **Acknowledgments:** The authors acknowledge the Center for Systems Science and  
267 Engineering (CSSE) at Johns Hopkins University for providing the COVID-19 data. We  
268 acknowledge E. Cheynet for providing the Generalized SEIR Epidemic Model (fitting and  
269 computation). This work was jointly supported by the National Science Foundation of China  
270 (41521004) and the Gansu Provincial Special Fund Project for Guiding Scientific and  
271 Technological Innovation and Development (Grant No. 2019ZX-06).

272

## 273 **References**

- 274 1. COVID-19 Data repository by the Center for Systems Science and Engineering (CSSE)  
275 at Johns Hopkins University 2020. <https://github.com/CSSEGISandData/COVID-19>.
- 276 2. Nicola, M. *et al.* The socio-economic implications of the coronavirus pandemic  
277 (COVID-19): a review. *Int. J. Surg.* **78**, 185–193 (2020).
- 278 3. World Health Organization (WHO). Coronavirus disease 2019 situation report 51 11th  
279 March 2020. *World Heal. Organ.* **2019**, 2633 (2020).
- 280 4. Petropoulos, F. & Makridakis, S. Forecasting the novel coronavirus COVID-19. *PLoS*  
281 *One* **15**, 1–8 (2020).
- 282 5. Linton, N. M. *et al.* Incubation period and other epidemiological characteristics of  
283 2019 novel coronavirus infections with right truncation: a statistical analysis of  
284 publicly available case data. *J. Clin. Med.* **9**, 538 (2020).
- 285 6. Tuli, S., Tuli, S., Tuli, R. & Gill, S. S. Predicting the growth and trend of COVID-19  
286 pandemic using machine learning and cloud computing. *Internet of Things* (2020)  
287 doi:10.1016/j.iot.2020.100222.
- 288 7. Wu, J. T., Leung, K. & Leung, G. M. Nowcasting and forecasting the potential  
289 domestic and international spread of the 2019-nCoV outbreak originating in Wuhan,  
290 China: a modelling study. *Lancet* **395**, 689–697 (2020).

- 291 8. Wang, H. *et al.* Phase-adjusted estimation of the number of coronavirus disease 2019  
292 cases in Wuhan, China. *Cell Discov.* **6**, 10 (2020).
- 293 9. Yang, Z. *et al.* Modified SEIR and AI prediction of the epidemics trend of COVID-19  
294 in China under public health interventions. *J. Thorac. Dis.* (2020)  
295 doi:10.21037/jtd.2020.02.64.
- 296 10. Godio, A., Pace, F. & Vergnano, A. SEIR Modeling of the Italian Epidemic of  
297 SARS-CoV-2 Using Computational Swarm Intelligence. *Int. J. Environ. Res. Public*  
298 *Health* **17**, 3535 (2020).
- 299 11. Huang, J. *et al.* Global prediction system for COVID-19 pandemic. *Sci. Bull.* (2020).
- 300 12. Huang J. and Y. Yi., Inversion of nonlinear dynamical model from the observation.  
301 *Science in China (B)*. 34, 1246-1251 (1991).
- 302 13. Huang J., Y. Yi, S. Wang, and J. Chou. 1993: An analogue-dynamical long-range  
303 numerical weather prediction system incorporating historical evolution. *Quarterly*  
304 *Journal of the Royal Meteorological Society*. 119, 547-565 (1993). DOI:  
305 10.1002/qj.49711951111.
- 306 14. Peng, L., Yang, W., Zhang, D., Zhuge, C. & Hong, L. Epidemic analysis of  
307 COVID-19 in China by dynamical modeling. *medRxiv* 1–18 (2020)  
308 doi:<https://doi.org/10.1101/2020.02.16.20023465>.
- 309 15. Cheynet, E. Generalized SEIR epidemic model (fitting and computation). *Github*  
310 (2020).
- 311 16. Huang, Z. *et al.* Optimal temperature zone for the dispersal of COVID-19. *Sci. Total*  
312 *Environ.* 139487 (2020) doi:10.1016/j.scitotenv.2020.139487.
- 313 17. Madsen, K., Nielsen, H. B. & Tingleff, O. *Methods for non-linear least squares*  
314 *problems*. (2004). doi:10.1155/2012/312985.
- 315 18. Kőházi-Kis, A. Relative effectiveness of the trust-region algorithm with precise second

- 316 order derivatives. **6**, 1–7 (2019).
- 317 19. Kim, C. Images of police using violence against peaceful protesters are going viral.  
318 <https://www.vox.com/2020/5/31/21275994/police-violence-peaceful-protesters-images>  
319 .
- 320 20. Rothenberg, C., Achanta, S., Svendsen, E. R. & Jordt, S. E. Tear gas: an  
321 epidemiological and mechanistic reassessment. *Ann. N. Y. Acad. Sci.* **1378**, 96–107  
322 (2016).
- 323 21. Parodi, S. M. & Liu, V. X. From containment to mitigation of COVID-19 in the US.  
324 *JAMA - J. Am. Med. Assoc.* **323**, 1441–1442 (2020).
- 325 22. Rocklöv, J. & Sjödin, H. High population densities catalyse the spread of COVID-19.  
326 *J. Travel Med.* **27**, 1–2 (2020).
- 327 23. McCloskey, B. *et al.* Mass gathering events and reducing further global spread of  
328 COVID-19: a political and public health dilemma. *The Lancet* vol. 395 1096–1099  
329 (2020).
- 330 24. Petersen, E. *et al.* Rapid spread of zika virus in the Americas - implications for public  
331 ealth preparedness for mass gatherings at the 2016 Brazil Olympic Games.  
332 *International Journal of Infectious Diseases* vol. 44 11–15 (2016).
- 333 25. Tosepu, R. *et al.* Correlation between weather and COVID-19 pandemic in Jakarta,  
334 Indonesia. *Sci. Total Environ.* **725**, (2020).
- 335 26. Tamerius, J. D. *et al.* Environmental predictors of seasonal influenza epidemics across  
336 temperate and tropical climates. *PLoS Pathog.* (2013)  
337 doi:10.1371/journal.ppat.1003194.
- 338 27. World Health Organization(WHO). Coronavirus disease (COVID-19) advice for the  
339 public.  
340 <https://www.who.int/emergencies/diseases/novel-coronavirus-2019/advice-for-public>.

- 341 28. Bai, Z. *et al.* The rapid assessment and early warning models for COVID-19.  
342 *Virologica Sinica* (2020) doi:10.1007/s12250-020-00219-0.
- 343 29. Kissler, S. M., Tedijanto, C., Goldstein, E., Grad, Y. H. & Lipsitch, M. Projecting the  
344 transmission dynamics of SARS-CoV-2 through the postpandemic period. *Science*  
345 (2020) doi:10.1126/science.abb5793.
- 346 30. Rainey, J. J., Phelps, T. & Shi, J. Mass gatherings and respiratory disease outbreaks in  
347 the United States – should we be worried? results from a systematic literature review  
348 and analysis of the national outbreak reporting system. *PLoS One* **11**, e0160378  
349 (2016).
- 350 31. Tomes, N. ‘Destroyer and teacher’: managing the masses during the 1918-1919  
351 influenza pandemic. *Public Health Reports* vol. 125 48–62 (2010).
- 352 32. Alexander Langmuir, M. D. Asian influenza in the United States. *Ann. Intern. Med.* **49**,  
353 483 (1958).
- 354 33. Prem, K. *et al.* The effect of control strategies to reduce social mixing on outcomes of  
355 the COVID-19 epidemic in Wuhan, China: a modelling study. *Lancet Public Heal.* **5**,  
356 e261–e270 (2020).
- 357 34. Shea, K. *et al.* Harnessing multiple models for outbreak management. *Science* (2020)  
358 doi:10.1126/science.abb9934.